Giant Organelle Vesicles Uncover Intracellular Membrane Mechanics and Plasticity

Alexandre Santinho[1], Maxime Carpentier[1], Mohyeddine Omrane[1], Abdou Rachid Thiam[1]*

[1] Laboratoire de Physique de l'École Normale Supérieure, ENS, Université PSL, CNRS, Sorbonne Université, Université de Paris, F-75005 Paris, France

*Correspondance to :
Abdou Rachid Thiam
Laboratoire de Physique Statistique,
Ecole Normale Supérieure,
PSL Research University,
75005 Paris Cedex 05, France
thiam@ens.fr

Abstract

Organelle plasticity facilitates numerous and diverse biological reactions. Unfortunately, it remains unclear how the membrane properties of organelles vary in space, time, or with the cell condition[1,2]. Currently, except for the plasma membrane[3,4], there is no means to reach and manipulate intracellular organelles for better knowing how they adapt to cues. Here, we generated and recovered functional giant organelle vesicles (GOVs), tens of μm sized, through osmotic[5–7] and lysis steps. GOVs were independent, or in contact, and had biophysical properties much lower than those of synthetic membranes. We found that Giant ER vesicles (GERVs) differed in properties depending on the organelle they were in contact with. Thus, force gradients exist within the ER, at least transiently, especially around contact sites. We also measured significant differences in biophysical properties between GERVs isolated from cells fed with different lipids or cholesterol. These properties gradually changed with lipid saturation and indicate how the ER membrane is remodeled depending on cues. Finally, to validate our conjectures, we tested whether GERVs could support lipid synthesis and droplet biogenesis, like the ER[10]. Indeed, GERVs synthesized neutral lipids, which, upon curvature induction[5], were condensed into a lipid droplet. These findings open new avenues for biophysics and biology.

Main

The reconstruction of elementary reactions of the cell has been a precious strategy to understand many cell biological processes[11]. Molecular biology, bottom-up cell biology, synthetic biology, and biophysical approaches have been major strategies. Yet, it remains extremely challenging to reconstitute organelles to study their properties, understand how they coordinate shape and function, how they spatially organize, and talk to each other[12,13]. The need to access this information has boosted the development of many microscopy imaging techniques[2,14,15]. This is well illustrated by the developing expansion microscopy field[16], offering an unprecedented spatial resolution by transforming nanometric distances to millimeters, but in fixed samples only. In contrast, classical subcellular fractionation assays give access to organelles[17] but the recovered nanometric fragments are unsuitable for manipulation. In comparison, the recovery of giant plasma membrane vesicles from blebbing cells allowed not only to carry on biophysical studies but also to reveal essential features of cell plasma membranes[18–20]. Here, we produced functional giant organelles and measured for the first-time membrane biophysical properties of purified giant organelles.

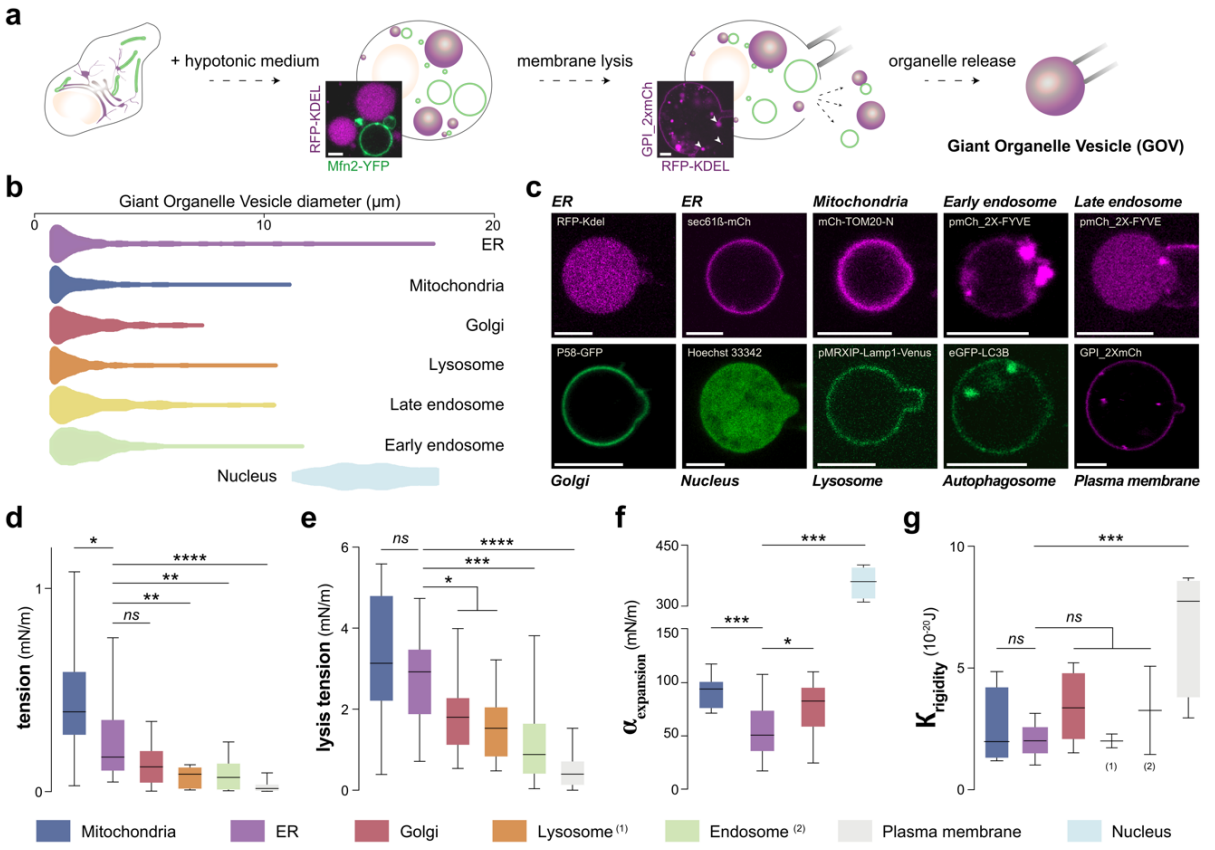

Figure 1 – Giant Organelles Vesicles' recovery and biophysical characterization

a. From left to right. Organelles reorganize into GOVs after hypotonic medium treatment**.** Confocal microscopy snap of a swollen COS-7 cells over-expressing both RFP-Kdel (marking ER volume) and Mfn2-YFP (mitochondrial membrane protein). Confocal microscopy snap showing the release of GERVs through a plasma membrane pore thanks to membrane suction generated with a micropipette. Cells were overexpressing GPI_2x-mCh (plasma membrane) and RFP-Kdel (ER). Scale bar, 5μm. Schematic representation of a collected Giant Organelle Vesicle. **b.** Violin frequency distribution plot of GOV's diameter. Only vesicles over 0.75μm were measured. **c.** Confocal microscopy snaps of collected GOVs. Fluorescence markers were used to report for a different type of GOVs: GERV (Giant ER Vesicle with RFP-Kdel or sec61ß-mCh signal); GMV (Giant Mitochondria vesicle with mCh-TOM20-N); GEEV (Giant Early Endosome Vesicle with a membrane signal of pmCh-2X-FYVE); GELV (Giant Late Endosome Vesicle with a volume signal of pmCh-2X-FYVE); GGV (Giant Golgi Vesicle with a P58-GFP membrane signal); GLV (Giant Lysosome Vesicle with a pMRXIP-Lamp1-Venus signal); GAV (Giant Autophagosome Vesicle with an eGFP-LC3B membrane signal); GPMV (Giant Plasma Membrane Vesicle with a GPI_2xmCh) and the nucleus identified with Hoestch 33342. Scale bars, 5μm. **d.** Plot of GOV's membrane tension. **e.** Plot of GOV's lysis tension. **f.** Plot of GOV's apparent area expansion modulus, $\alpha_{expansion}$. **g.** Plot of GOV's bending rigidity. (Fig. 1d-g; Median, 1th and 3rd quartiles, max and min values. **** $p < 0.0001$; *** $p < 0.001$; ** $p < 0.01$; * $p < 0.05$. See Supplementary Data Table 1 for statistical analysis and data sets).

To generate intracellular organelles with a size over 3μm, which is the minimum size suitable for classical micromanipulation experiments[21], we subjected COS-7 cells to a hypotonic buffer[5–7] (Fig. 1a). Following this process, cells became spherical and tenser (Extended Data Fig. 1a). This led to the swelling of bilayer-

encircled organelles only (Extended Data Fig. 1b-h). Except for peroxisomes[6], micrometric GOVs were generated (Fig. 1b, Extended Data Fig. 1i). The size of giant ER vesicles (GERVs), up to 18μm, was significantly larger than organelles except for the nucleus (Fig. 1b, Extended Data Fig. 1i). Since the swelling process should theoretically minimize the surface-to-volume ratio of the organelles, we assumed that the GOVs size could be modified by tuning this ratio before swelling. To test this, we overexpressed Climp-63, promoting ER sheets over tubules[22] (Extended Data Fig. 2a). Swelling led to the formation of GERVs occupying the entire cell cytosol, squeezing all the rest to the periphery (Extended Data Fig. 2b,e-g). Similarly, nocodazole treatment, which disrupts microtubules and promotes more ER sheets (Extended Data Fig. 2c), also increased GERVs' size (Extended Data Fig 2d,e-g). Finally, the overexpression of Mitofusin-2 increased the size of giant mitochondrial vesicles (GMV) (Extended Data Fig. 2h-j). This data confirms that GOV sizes are dependent on the organelle's native shape.

Following the swelling process, we captured swollen cells with a micropipette. We then increased its plasma membrane tension until it broke (Fig. 1a, Extended Data Fig. 3a). Giant organelle vesicles (**GOVs**), were then delivered spontaneously and isolated (Fig. 1c). This strategy permitted to break one cell at a time (Extended data Fig. 3a). However, by applying aspiration and refill cycles with a pipette to the bulk medium, many cells were lysed and many GOVs were freed (Extended Data Fig. 3b). This approach was effective on COS-7, HeLa, Huh7, HEK, and fibroblasts which are very different cell types (Extended Data Fig 3c-j). Thus, our approach applies to many cell types. We took advantage of this unique and unprecedented opportunity to manipulate single GOVs to determine their biophysical properties (Fig. 1d-g). For the different GOVs, we determined when it was possible (Supplementary Text) the surface tension, the lysis tension, their apparent area expansion modulus ($\alpha_{expansion}$), and their bending rigidity (K) (Fig 1d-g, Extended Data Figure 4a-o, Methods).
The initial tension of our generated plasma membrane vesicles was 0.02±0.01mN/m (Fig. 1d, Extended Data Fig. 4a), close to the value from giant plasma membrane vesicles (GPMVs), or cells subjected to hypotonic shocks[14,23]. The plasma membrane was followed by early endosomes (0.07±0.05mN/m) and lysosomes (0.08±0.03mN/m). Mitochondria had the highest value (0.44±0.11mN/m), then the ER (0.24±0.08mN/m) and the Golgi (0.14±0.04mN/m) (Fig. 1d). These initial surface tensions of GOVs were not the native ones for the organelles, but they probably reflect differences in native tensions between the organelles and their luminal osmolarity. We then measured the GOVs lysis tension (Fig 1e, Extended Data Figure 4b), indicating how much the membrane sustains stretching. The lysis tension of the GOVs, between 1.1±0.4mN mN/m and 3.3±0.7mN/m (Fig. 1e), overall followed the same trend as the initial tensions. Plasma membrane vesicles, which were subjected to the extraction protocol, had the lowest lysis tension (0.5±0.2mN/m) (Figure 1e). Finally, GOV's lysis tensions were much lower than for Giant Unilamellar Vesicles (GUVs) (8mN/m)[21]. This reveals considerable contributions not recapitulated in synthetic membranes. Regarding the apparent area expansion modulus, the nucleus had the highest modulus (356±61mN/m), followed by mitochondria (~92±13mN/m), the Golgi (~78±15mN/m), and the ER (~55±12mN/m) (Fig. 1f, Extended Data Fig. 4c-j). These values are significantly lower than that of dioleoyl phosphatidylcholine GUVs (~ 200mN/m)[21,24], likely because of the contribution of membrane proteins in GOVs. Regarding the bending rigidity, the ER, lysosomes, and mitochondria, had similar and the lowest rigidities (~ 6 k_BT). They were followed by endosomes and the Golgi (~ 9 k_BT). Finally, all GOVs exhibited lower rigidities than plasma membrane vesicles (17 k_BT), close to the measured rigidity for GPMVs and GUVs[23]. These data indicate significant variations in the mechanical properties across organelles and provide insights into the spectrum of intracellular forces required to their shaping processes. Also, the rigidities seem to gradually increase across organelles of the secretory pathway (Figure 2d) while both the initial and lysis membrane tensions seem to follow the opposite (Figure 2a,b).

In the previous measurements, we cannot exclude overexpression artifacts, since the overexpressed proteins may alter the membranes' mechanics. When we overexpressed Sec61ß or Sec22, which are ER membrane proteins, instead of KDEL, which labels the ER lumen, we found that GERVs had similar properties (Extended Data Figure 4o-q), indicating that, at least for the ER, the overexpression did not alter the mechanical properties.

Next, we did not recover only independent GOVs but also populations of GOVs developing bipartite (Fig. 2a, Extended Data Fig. 5a-d), tripartite or more contacts (Extended Data Fig. 5e-g). GERVs were central to these contact, likely reflecting the importance of the ER membrane, as the largest organelle[13] in contact with all others[12]. We decided to measure the spatial ER surface tension distribution based on these contacts (Fig. 2c). Thus, we selected KDEL-based (or ERox) GERVs developing contacts majorly with one type of GOV (Fig. 2b, Extended Data Figure 5h-o, 6a-i, Methods). GERVs in contact with lysosomes had the highest initial bilayer tension (0.55 mN/m), followed by those in contact with both Golgi or Lipid Droplets (0.37mN/m) and mitochondria (0.31mN/m) (Fig. 2c). These tensions are larger than that of single GERVs (0.24mN/m). In contrast, GERVs in contact with peroxisomes and the nucleus, i.e., the nuclear ER, had lower tensions (0.13mN/m). Regarding the lysis tensions, it was slightly higher for GERVs in contact with lysosomes and lipid droplets (3.5mN/m) than for

single GERVs (2.7mN/m) (Figure 2c). GERV-Golgi had similar lysis tension than individual GERVs when GERVs in contact with the nucleus, peroxisomes, and mitochondria had lower lysis tensions (~2mN/m).

These data suggest the existence of surface tension gradients, at least transiently, across the ER membrane. Threefold differences in tension could occur within the ER, between the nuclear-ER and ER in contact with lysosomes. Since the ER is a contiguous network, the maintenance of a tension gradient could be a mechanism shaping the membrane or producing active flows of proteins and lipids, toward specific ER regions. Finally, ER regions in contact with lipid droplets, storing neutral lipids, appeared to significantly sustain larger stretching than the nuclear ER, involved in proteins synthesis. Such difference in tension may also reflect discrepancies in the spatial biochemical composition of the ER membrane. For instance, ER membranes in contact with lipid droplets (LDs) could locally bear more neutral lipids, which can strongly alter its mechanics[5,24].

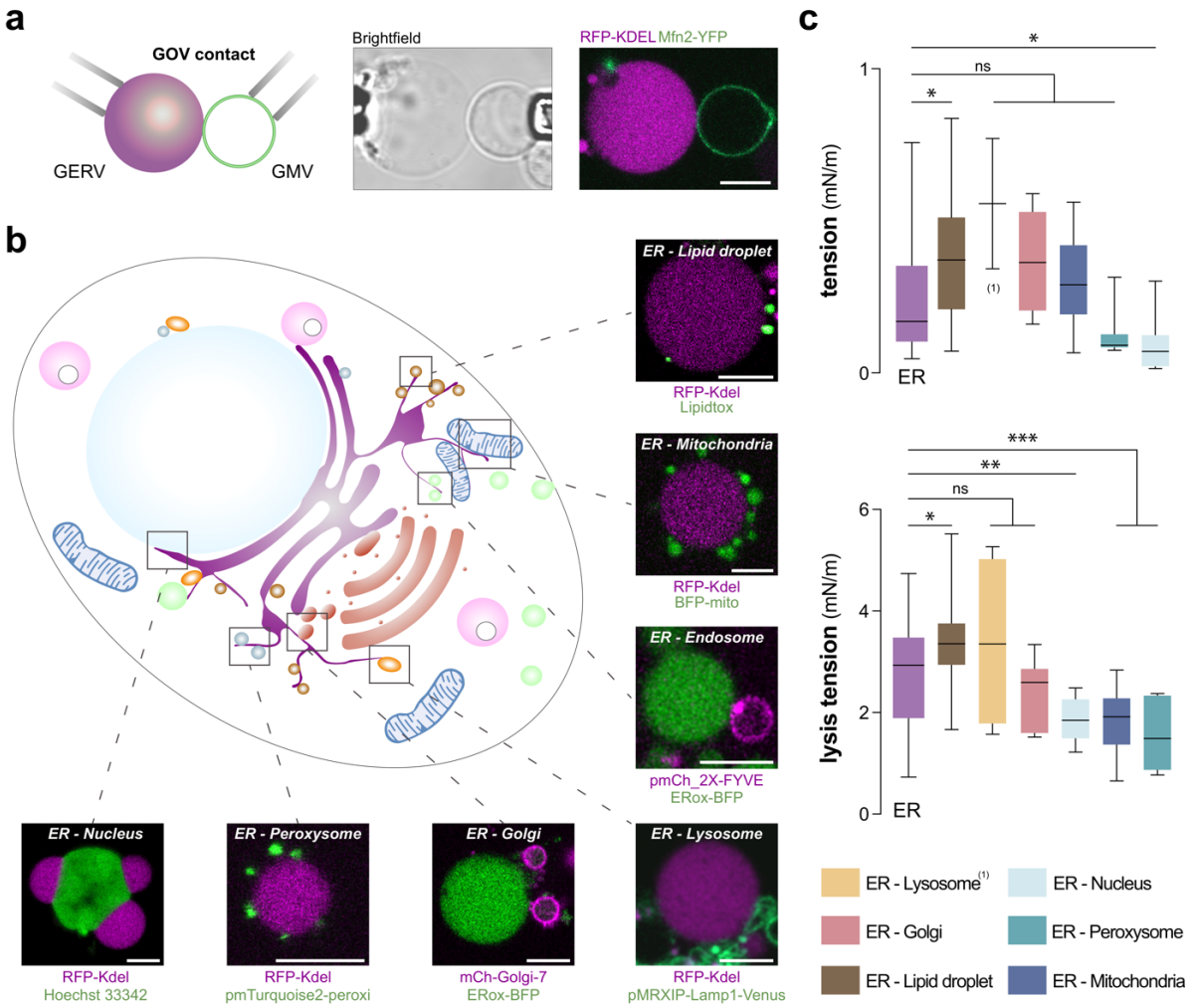

Figure 2 – Mapping the biophysical properties of the ER at its contact regions

a. Left: Schematic representation of an isolated GERV-GMV contact held with micropipettes. **Right:** Confocal microscopy snap of an isolated KDEL-based GERV recovered in contact with a Mfn2-based GMV. For imaging, the GOVs were immobilized with micropipettes. Scale bar, 5μm. **b.** Schematic representation of a cell where organelles contact between ER and others are underlined. For each of these contacts, a confocal microscopy snap shows the recovery of a GERV contacting other GOVs. Fluorescent proteins used to visualize contacts are indicated below each snap. **c. Top:** Plot of the initial membrane tensions of based GERVs contacting other GOVs. **Bottom.** Plot of the lysis tensions of KDEL-based GERVs contacting other GOVs (Only RFP-KDEL and ERox-BFP volume markers were used to not alter membrane properties of the ER). (Fig. 2c; Median, 1th and 3rd quartiles, max and min values. **** $p < 0.0001$; *** $p < 0.001$; ** $p < 0.01$; * $p < 0.05$. See Supplementary Data Table 2 for statistical analysis and data sets).

Membrane properties, structure, and function strongly rely on lipid composition, saturation, or cholesterol[25–29]. We explored the extent to which these lipids alter the properties of the ER. We fed cells with fatty acids with different saturations, from the unsaturated palmitic acid to the polyunsaturated arachidonic acid, mixed with

oleic acid (1:1), or cholesterol (Fig. 3a, Methods). These lipids were supplied for 24hrs before GERVs were made. The impact of palmitic acid and cholesterol was consistently predominant (Fig. 3b-d). They noticeably increased the lysis tensions and the area expansion modulus compared to control GERVs (Fig. 3b-d). In striking contrast, linoleic, linolenic, and arachidonic decreased the tensions slightly but drastically decrease the area expansion modulus (Fig. 3b-d). These parameters changed by almost 4 folds between palmitic and arachidonic acids, highlighting the extent to which the ER has to act to control its lipid saturation level[27] to preserve its mechanical fingerprint. These data reveal the extent of ER properties' changes when these lipids accumulate, e.g., during specific metabolic states or ER stresses, or from diet. Other lipids such as ceramides or ether lipids could be expected to significantly alter these properties as well. Finally, we wondered whether the changes in properties by fatty acid feeding could be restored by starvation. For oleic acid, often used to induce lipid droplets, we found that all GERVs' properties were comparable to the unfed condition, except for the apparent area expansion modulus (Extended Data Fig 7a-c). Therefore, the ER membrane properties may not be completely rescued following feeding-starvation cycles.

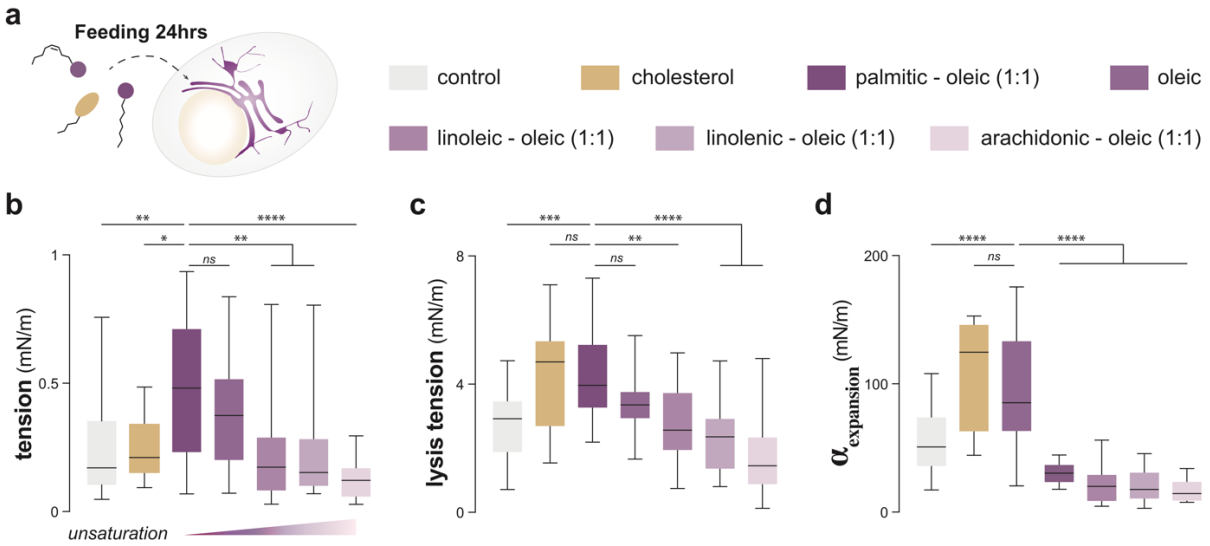

Figure 3 - Metabolic state and ER properties
a. Cell feeding protocol. Once the cells were transfected, they are subjected to a loading of a combination of carboxylic acids or cholesterol. **b.** Plot of the initial membrane tensions of GERVs after 24hrs cell feeding. **c.** Plot of the lysis tensions of GERVs after 24hrs cell feeding. *(Fig. 3b-d;* Median, 1th and 3rd quartiles, max and min values. **** $p < 0.0001$; *** $p < 0.001$; ** $p < 0.01$; * $p < 0.05$. See Supplementary Data Table 3 for statistical analysis and data sets).

To further support our conclusions on the ER properties based on our analysis from GERVs, we asked whether GERVs could reproduce elementary biochemical and biophysical reactions of lipid synthesis and lipid droplet biogenesis. We made GERVs and supplied them with diacylglycerol, oleyl-CoA, containing 1% NBD-Oleoyl-CoA (Methods) to fluorescently visualize neutral lipid synthesis[5]. We observed that GERVs' membrane acquired the NBD-fluorescence over time (Fig. 4a, Extended Data Fig. 8a,b). This increase in fluorescence is likely due to the synthesis of fluorescent triglycerides[5], since GPI_2x-based GPM-like vesicles, which do not possess the triacylglycerol synthesis enzymes, almost lacked the fluorescence (Fig. 4b, Extended Data Fig. 8c-e). This result suggests that GERVs keep lipid synthesis functions. Accordingly, when we overexpressed DGATs-eGFP, converting diacylglycerol to triacylglycerol, and used LipidTox to stain neutral lipids, DGAT-eGFP-positive GERVs had more LipidTox signals than other GOVs (Fig. 4c,d, Extended Data Fig. 8). Since the presence of free triglyceride molecules alters the bilayer properties[24], we measured the biophysical parameters of triglyceride-containing GERVs and confirmed changes in their membrane mechanics (Extended Data Fig. 8h-k). Finally, we determined whether the accumulated neutral lipids could be assembled into lipid droplets. The condensation of free triglyceride molecules into lipid droplets is catalyzed by membrane curvature and seipin[30–32], an integral ER membrane protein enriched in curved regions[5,33]. Thus, we overexpressed YFP-seipin, generated GERVs, on which the proteins were mobile (Fig. 4e, Extended Data Fig. 9a-d). By pulling a tube, we found that seipin was enriched in the curved region as compared with Sec61ß[5] (Fig. 4f). Next, we triggered the synthesis of neutral lipids as previously (Fig. 4a). By inducing curvature, we observed the appearance of LipidTox puncta's colocalizing with seipin (Fig. 4g, Extended Data Fig. 8e,f), indicating that seipin catalyzed or controlled the condensation of the triglycerides into nascent lipid droplets[30,34–36]. Altogether, these data demonstrate that GERVs preserve features of lipid synthesis and organelle biogenesis of the ER.

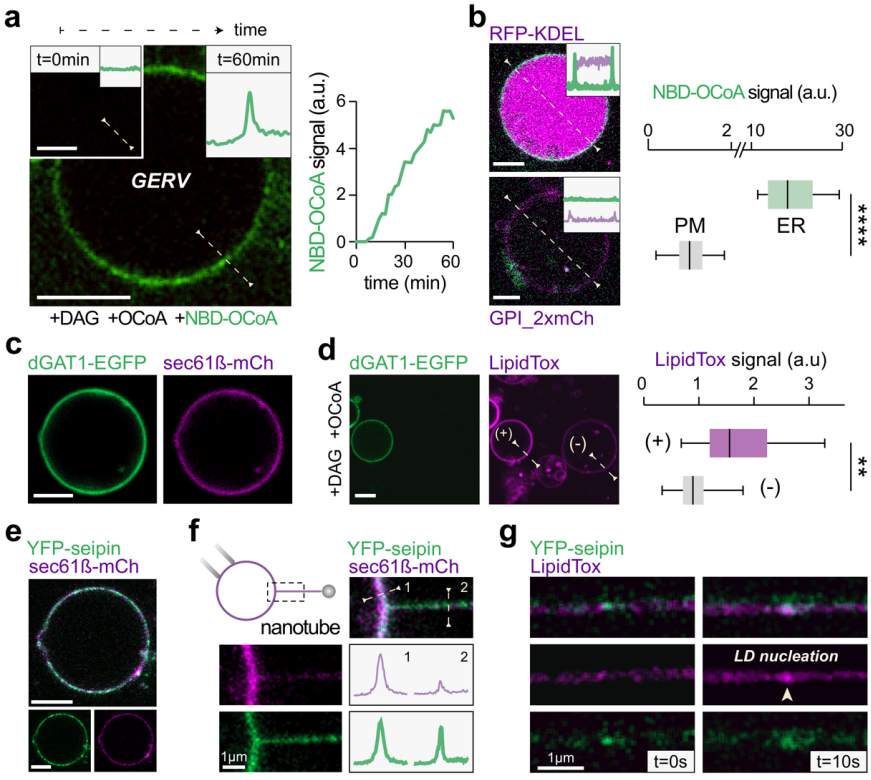

Figure 4 - GERVs are functional, synthesize neutral lipids, and support lipid droplet biogenesis.

a. Left. Confocal microscopy snap of a GERV. The GERV is supplied with Oleoyl-CoenzymeA (OCoA) complemented with NBD-Oleoyl-Coenzyme A (NBD-OCoA) and diacylglycerol (DAG) at 37°C during 1h. Fluorescence signals at the top right corners of snaps correspond to the dotted line profile drawn on confocal snaps. Scale bar, 5μm. **Right.** Plot of the NBD-OCoA fluorescence signal in the GERV membrane during the OCoA supply experiment increases linearly with time reporting for lipid synthesis. **b. Left.** After 1hr of OCoA supply (same conditions as Figure 4a), both KDEL-based GERV and GPI-based GPMV were imaged in confocal microscopy. Fluorescence signals at the top right corner correspond to the dotted line profile drawn on confocal snaps. Scale bars, 5μm. **Right.** Plot of the NBD-OCoA fluorescence signal in GERVs and GPMVs after 1hr of feeding. **c.** GERVs were isolated from COS-7 cells overexpressing the dGAT1-EGFP enzyme. **d. Left.** Then, the isolated vesicles were subjected to the same feeding conditions as in Figure 4a. LipidTox was added to report for membrane hydrophobicity. Scale bars, 5μm. **Right.** Box and whiskers plot of the LipidTox fluorescence in vesicles positive for dGAT (+) or negative (-). **e. Left.** Confocal microscopy snap of an isolated seipin/sec61ß-based GERV. Scale bar, 5μm **Top.** Schematic representation of a membrane nanotube extraction from a GERV. The rectangular shape indicates our ROI. **Right.** Confocal microscopy snap of the nanotube extracted from a seipin/sec61ß-based GERV. Fluorescence profiles are drawn perpendicular to the membrane both in the flat region (1) and in the nanotube (2). **f.** Confocal microscopy snaps of a nanotube extracted from a seipin-based GERV. LipidTox fluorescence is monitored to visualize the formation of a nascent oil lens in the tube. The arrows indicate an oil lens growing just after tube extraction (t=0s). (Fig. 4b,d; Median, 1th and 3rd quartiles, max and min values. **** $p < 0.0001$; *** $p < 0.001$; ** $p < 0.01$; * $p < 0.05$. See Supplementary Data Table 4 for statistical analysis and data sets).

We surmise that other GOVs also kept functionalities of the organelles they derived from.

Organelles possess a wide range of functions, granting to cells their title of the smallest functional unit in the living world. Through the novel technique we developed, we are now capable for the first time of physically touching almost all organelles. This groundbreaking technique promises a bright future for life science and medicine, as we are now able to delve deeper biophysical and biological mechanisms of organelles. This is for example well illustrated by our discovery of the mechanical heterogeneity in the ER spatial membrane, at contact sites. We foresee the recovery of organelles from healthy vs. diseased tissues as a future approach for understanding the onset of some diseases based on variations in the organelles' biophysical properties. Such diverse assets of our strategy represent a big potential for the future of cell biology, biophysics, and clinics.

Methods

Cell culture

COS-7, HeK, HeLa, and Huh7 cells were maintained in High Glucose (4.5g/l) with stabilized Glutamine and with Sodium Pyruvate Dulbecco's modified Eagle's Medium (DMEM) (Dutscher) supplemented with 10% fetal bovine serum and 1% penicillin/streptomycin (GibcoBRL). Fibroblast cells were maintained in the same conditions but with 1g/L of glucose. Cells were cultivated 48h at 37°C with 5% CO_2.

To induce feeding conditions and lipid droplet formation (Fig. 3), COS-7 cells were incubated for 24h with DMEM supplemented with fatty acids conjugated to bovine serum albumin (BSA) (1% vol/vol). Finally, feeding conditions (Fig. 3) were 200µM of oleic acid; 200µM of palmitic acid and 200µM of oleic acid; 200µM of linoleic acid and 200µM of oleic acid; 200µM of linolenic acid and 200µM of oleic acid; 200µM of arachidonic acid and 200µM of oleic acid. To induce cholesterol-enriched lipid droplet formation, 0,5% v/v of 400µM of cholesterol solubilized in ethanol solution were added to the culture media.

To induce starvation conditions (Extended Data Fig. 7), COS-7 cells were incubated in EBSS, calcium, magnesium, rouge de phenol (ThermoFisher # 24010043).

Cell transfections and plasmids

Cells were seeded in MatTek 3.5mm coverslip bottom dishes (MatTek Corp. Ashland, MA) for 16h before transfections. Cells were transfected with indicated plasmid using jetPEI transfection reagent (PolyPlus #101- 10N). Cells were transfected with different plasmids fused with fluorescent protein constructs 24h before giant organelles collection. Here is the list of the used plasmids.

- mCh-Climp63 was a gift from Gia Voeltz (Addgene plasmid # 136293 ; http://n2t.net/addgene:136293 ; RRID:Addgene_136293).
- Both RFP-KDEL and P58GFP are a gift from Catherine L. Jackson from Jacques Monod Institute - UMR 7592 CNRS – Paris university.
- Both dGAT1-EGFP and dGAT2-EGFP are gifts from professor Robert YANG School of Biotechnology and Biomolecular Sciences, the University of New South Wales, Sydney, NSW 2052, Australia.
- ERoxBFP was a gift from Erik Snapp (Addgene plasmid # 68126 ; http://n2t.net/addgene:68126 ; RRID:Addgene_68126).
- mCh-Sec61ß was a gift from Gia Voeltz (Addgene plasmid # 49155 ; http://n2t.net/addgene:49155 ; RRID:Addgene_49155) (Zurek et al., 2011).
- pEGFP Sec22b was a gift from Thierry Galli (Addgene plasmid # 101918 ; http://n2t.net/addgene:101918 ; RRID:Addgene_101918) (Petkovic et al., 2014).
- Seipin human EGFP, pSH-EFIRES-B-Seipin-miniIAA7-mEGFP was a gift from Elina Ikonen (Addgene plasmid # 129719 ; http://n2t.net/addgene:129719 ; RRID:Addgene_129719) (Li et al., 2019)
- mCherry-TOMM20-N-10 was a gift from Michael Davidson (Addgene plasmid # 55146; http://n2t.net/addgene:55146; RRID: Addgene_55146)
- Mfn2-YFP was a gift from Richard Youle (Addgene plasmid # 28010 ; http://n2t.net/addgene:28010 ; RRID:Addgene_28010) (Karbowski et al., 2002).
- Mito-BFP was a gift from Francesca Giordano Institute for Integrative Biology of the Cell(I2BC), CEA, CNRS, Paris-Sud University, Paris-Saclay University, Gif-Sur-Yvette Cedex 91198, France.
- KDE-GFP (Dipeptidyl peptidase IV in which the extracellular domain had been replaced by the GFP sequence to restrict protein localization to the Golgi apparatus) was a gift from Professor Christian Poüs (Paris-Sud University, France)
- mCh-Golgi-7 was a gift from Michael Davidson (Addgene plasmid # 55052 ; http://n2t.net/addgene:55052 ; RRID:Addgene_55052)
- pmCherry-2xFYVE was a gift from Harald Stenmark (Addgene plasmid # 140050 ; http://n2t.net/addgene:140050 ; RRID:Addgene_140050)
- pMRXIP Lamp1-Venus was a gift from Noboru Mizushima (Addgene plasmid # 89937; http://n2t.net/addgene:89937; RRID: Addgene_89937) (Tsuboyama et al., 2016)
- GPI_2xmCherry was a gift from Salvatore Chiantia (Addgene plasmid # 127812 ; http://n2t.net/addgene:127812 ; RRID:Addgene_127812) (Dunsing et al., 2018)
- eGFP-LC3B adenovirus was kindly provided by Sharon Tooze (London Research Institute, UK) and was amplified in QBI-HEK 293A cells and purified on a cesium chloride gradient.
- pmTurquoise2-Peroxi was a gift from Dorus Gadella (Addgene plasmid # 36203 ; http://n2t.net/addgene:36203 ; RRID:Addgene_36203)

Fluorescent probes

Cell nucleus were probed with Hoechst 33342 Solution (0.1% v/v; Cat# 62249 *ThermoFisher*). Both organelle membranes and lipid droplets were tagged with HCS LipidTox™ Deep Red Neutral Lipid Stain, , (0.1% v/v;

Cat# H34477 Thermo fisher); or AUTOdot, (0.1% v/v; Cat# SM1000a abcepta).

GOVs production and size distribution
After transfection, cells were incubated for 24h until 70-80% confluence. Cells were then transferred into a hypotonic culture media DMEM: H2O (5:95% v/v) at pH 7.4, at 37°C, 5% CO2, to induce GOVs. Confocal microscopy Z-stack was made on entire swollen cells for GOV's diameter distribution studies. (Fig. 1, Extended Data Fig. 1,2). We only considered organelles vesicles over 0,75µm in diameter for size distribution measurements. Size distributions are shown as frequency distribution by using GraphPad Prism software and the violin plot settings (Fig. 1) or histogram plot (Extended Data Fig. 1). See

Nocodazole treatment
To induce larger GOVs (Extended Data Fig. 2), COS-7 cells were incubated with a culture medium containing nocodazole (Cat#487928 from Calbiochem) (2.5µg/ml) for 1 hour at 37°C. Cells were then imaged after swelling in the hypotonic media.

Micro-manipulation
Micropipettes were used to manipulate cells and GOVs. Micropipettes were made from capillaries (1.0 OD, 0.58 ID, 150 L (mm)), 30-0017 GC100-15b; Harvard Apparatus, Holliston, MA) with a micropipette puller (model P-2000; Sutter Instruments). The pipettes were subjected to plasma cleaner and treated with a solution of mPEG5K-silane (Cat #JKA3037 from Merck) at 3mg/mL in ethanol: H_2O (95:5 v/v) solution. Then, micro-pipettes were cleaned into DMEM: H_2O (5:95 v/v). Micromanipulation robot (TransferMan 4r) was provided by Eppendorf (Hamburg, Germany). Before micromanipulation, biological samples were injected on a cover-slip glass plate, pre-treated with BSA, and cleaned with DMEM: H_2O (5:95 v/v).

GOVs extraction protocols
On one hand, once swollen, cells were caught and suctioned with micropipettes to increase their membrane tension which resulted both in plasma membrane rupture and the GOVs release (Fig. 1, Extended Data Fig. 3a). On the other hand, swollen cells in the bulk were subjected to pipette (ID : 1mm) back and refill cycles. Then, GOVs were visualized under microscopy (Extended Data Fig 3b-j).

GOVs membrane tension measurements
Using Laplace's law, and the measurement of the pipette inner radius (R_p), GOV radius (R_{GOV}), and suction pressure ΔP, the surface tension γ of the interface was calculated as follows:

$$\gamma = \frac{\Delta P . R_p}{2(1 - {R_p}/{R_{GOV}})}$$

See Extended Data Fig4a.
The suction was carried out using a syringe. The resulting pressure was measured with a pressure transducer (DP103; Validyne Engineering, Northridge, CA). The output voltage was monitored with a digital voltmeter (FLUKE 16 multimeter) which gave us a pressure measurement sensibility of 1Pa. The pressure transducer was calibrated before the experiments.

GOVs lysis tension measurements
We used the micropipette aspiration technique and a manometer (PCE P15) to measure the suction pressure ΔP (1) during GOV's lysis tension measurements. Thanks to a slight aspiration, a bilayer tongue was first sucked into the micropipette. The aspiration was then increased at a constant rate of approximately 10mbar/min, causing a proportional increase in the bilayer surface tension (see the section below). At a certain tension, the GOV ruptured because of a pore opening in its membrane. The lysis tension was taken as the higher tension reached just before bilayer rupture.

GOVs apparent area expansion modulus measurements
GOVs were gently captured with a micropipette. Then, aspiration in the micropipette was slowly increased to obtain multiple values of membrane tension (only for membrane tension above 0,75mN/m, ~ 20 seconds were let between each increment of tensions to reach equilibrium). For each value of applied bilayer tensions, variation of both membrane tongue length (in the micropipette) and radius of the GOV were measured (Extended Data Fig. 4c,d). This allowed to determine both the exact surface area A_γ (2) of a GOV for a given membrane tension γ and its variation of area ΔA_γ (3) between the initial membrane tension γ_0 and the current one γ (See Supplementary Text and Extended Data Fig. 10 for more details), (Olbrich et al., 2000) :

$$A_\gamma = 2\pi.\left(R_{GOV,\gamma}^2\left[1 + \sqrt{1 - ({R_p}/{R_{GOV},\gamma})^2}\right] + R_p.L_{p,\gamma}\right)$$

And,

$$\Delta A_\gamma = 2\pi\left(R_{GOV,\gamma}^2\left[1 + \sqrt{1 - ({R_p}/{R_{GOV},\gamma})^2}\right] - R_{GOV,\gamma_0}^2\left[1 + \sqrt{1 - ({R_p}/{R_{GOV},\gamma_0})^2}\right] - R_p(L_{p,\gamma} - L_{p,\gamma_0})\right)$$

Where $L_{p,\gamma}$, L_{p,γ_0}, R_p, $R_{GOV,\gamma}$ and R_{GOV,γ_0} are respectively the bilayer tongue length in the micropipette for the initial tension γ_0 and a given tension γ, the inner pipette radius, and the GOV radius both at tension γ and initial tension γ_0. The applied bilayer tension γ was then plotted against the relative surface area variations of the GOV's bilayer ${\Delta A_\gamma}/{A_{\gamma,0}}$ (Extended Data Fig. 4e). For tensed membrane regimes (tension above 0.75mN/m), membrane fluctuations

were negligible and the bilayer tension γ can be linked to the surface area variation $\Delta A_\gamma / A_{\gamma,0}$ by the apparent area expansion modulus ($\alpha_{expansion}$):

$$\alpha_{expansion} = \frac{\gamma}{\Delta A_\gamma / A_{\gamma,0}}$$

Therefore, the slope of the bilayer tension against the area relative variation, extracted with linear regression, gave us the apparent area expansion modulus of the membrane ($\alpha_{expansion}$).

GOVs bending modulus measurements

To determine the bending moduli, we used the same method as in Rawicz & al., 2000. Like in the previous section, we determined area variations of GOVs for different membrane tensions, but, in the range of minuscule bilayer tensions γ < 0.5mN/m. To do so, we had to decrease the initial membrane tensions of GOVs. Thus, they were transferred into a DMEN: H_2O (33:67) diluted media. Then, the GOVs were caught and we spanned three orders of magnitudes of membrane tensions (0.001 mN/m to 0.1mN/m). In these regimes, vesicle area relative variations increase linearly with ln(γ) (Extended Data Fig. 4m,n). The slope λ of this linear curve was obtained thanks to linear regression for ln(γ) with values which were between -6 and -2. Then, λ was multiplied by $K_BT/8\pi$ (where K_B and T are respectively the Boltzmann constant and the temperature) to obtain the bending moduli κ (Extended Data Fig. 4n).

Sampling of GOVs for biophysical properties

Our GOV samples for membrane properties measurements were chosen with a radius between (2µm and 8µm). To reduce the uncertainty of our measurements, we measured membrane properties only for GOVs which were following this ratio: $R_p / R_{GOV} < 0.5$ (where R_p is the pipette inner radius and R_{GOV} the GOV radius). Note that for Fig. 1d-g, mCherry-TOMM20-N-10 based GMVs, RFP-KDEL based GERVs, P58GFP based GGVs, pMRXIP Lamp1-Venus based GLVs, pmCherry-2xFYVE based GEEVs, and GPI_2xmCherry based GPMVs were used to measure biophysical parameters. Note that for GERV-contacts (Fig. 2b,c), only KDEL or ERox based-GERV (volume marker to avoid the effect of ER membrane proteins) exhibiting contact with at least two other organelles of the same type were chosen. For Fig. 3 and Extended Data Fig. 7a-c & 8h-k, only KDEL-based GERVs were used to measure biophysical properties.

Lipid supply to GERVs

A supply mixture of diolein (Cat# D0138 from Merck) at 8mM, 18:1 (n9) CoenzymeA (Cat# 870719P from Avanti) at 2mM and 18-NBD 18:1 Coenzyme A (Cat# 810229 from Avanti) at 20µM was prepared. These molecules were mixed with BSA (0,5%) in hypotonic culture media (DMEM: H_2O 5:95). GOVs were incubated for 1hr at 37°C and 5% CO_2 and supplied with the mixture at 2.5% v/v. Finally, final concentrations are 200µM, 50µM, and 0,5µM respectively for the diolein, OCoA, and NBD-OCoA. The incorporation of OCoA into triglycerides in GERV has been monitored thanks to the fluorescence signal of NBD-OCoA (Fig. 4a, Extended Data Fig. 8a,b). Snaps were taken every 2 minutes and the fluorescence was analyzed by drawing an orthogonal line profile (10 pixels thick) to the GERV membrane, always at the same position. Then, each peak of fluorescence was registered (Fig. 4a). Same quantifications were made (Fig. 4b, Extended Data Fig. 4c-e). After1hr of OCoA supply, the hydrophobicity of GERVs' membrane was quantified thanks to LipidTox addition (0.05% v/v). (Fig. 4c,d, Extended Data Fig. 8f,g).

Nanotube extraction from GERVs and protein partitioning

Nanotubes were pulled from GERVs thanks to a micropipette. The GOV was gently captured by one of the two micro-pipettes. The over micropipette was slowly moved toward the GOV. Upon contact, some PEG silane coverture defects on the micropipette glass surface allowed the sticking of the GERV membrane. Finally, after adsorption of the GERV membrane on the pipette, a nanotube was extracted from the GERV by removing slowly the micropipette in the opposite direction of the GOV. Fluorescence profiles (10 pixels of thickness) were drawn perpendicular to the GERV membrane and the extracted nanotube (Fig. 4f) to quantify protein partitioning between flat and curved regions.

Nucleation of oil lens in GERVs

Following the lipid supply protocol in seipin-based GERVs (section above). LipidTox was added (0.05% v/v) in the solution to visualize the hydrophobic region in the membrane to report for neutral lipids condensation. Thanks to the nanotube extraction protocol, a curvature is rapidly induced on the GERV membrane. YFP-seipin and LipidTox signals are monitored in the nanotube thanks to living confocal microscopy. The nucleation of an oil nano-droplet and its interaction with seipin is finally visualized in the nanotube thanks to the LipidTox signal (Fig 4g, Extended data Figure 9e,f).

FRAP experiment in GERVs

Fluorescence recovery after photobleaching (FRAP) experiments were performed by bleaching a part of the GOV bilayer (Extended Data Fig. 9c,d). Fluorescence proteins were bleached, and then, the recovery of both signals was monitored. The FRAP curves were normalized by the fluorescence before bleaching GOVs and just after the bleach in the region of interest. To avoid losses of signals during FRAP, we re-normalized our recovery curve with the fluorescence signals in the

non-bleached regions of the GOV. GraphPad Prism was used to fit the FRAP recovery curve with a nonlinear regression and the exponential ‘‘one-phase association model.’’.

Confocal microscopy imaging

All micrographs were made on a Carl ZEISS LSM 800. GFP fluorescence was excited at 488 nm, and emission was detected between 510 and 550 nm, while mCherry tagged protein fluorescence was excited at 540nm, and emission was detected between 580 and 650 nm. Deep red fluorescence was excited at 640nm and was detected above 650nm. BFP fluorescence was excited at 420nm and detected below 500nm. All fluorescence signals were analyzed with ImageJ.

Statistical analysis (See Supplementary Data Table 1-9)

Data Sets

Sample analysis (sample size, test details, descriptive statistics, data sets) are available in the Supplementary Data Table *Excel* file.

Statistical Tests

The statistical analyses were made with GraphPad Prism 7.0a For statistical analysis, each data set distribution was first submitted to a Shapiro-Wilk Normality test to control sample Gaussian distributions. First, if there were only two conditions to compare per plot, and if their distributions were Gaussians ($P > 0.05$), samples were compared with a parametric unpaired t-test with Welch’s correction. If not ($P < 0.05$), they were compared with a non-parametric Mann Whitney test. Then, if there were more than two conditions to compare per plot, and if all conditions were positive for normality ($P > 0.05$), data were compared with parametric, multiple comparison, uncorrected Fisher’s LSD tests. If at least, one condition was not positive for normality ($P < 0.05$), all conditions were compared with a non-parametric, uncorrected Dunn’s test. For all tests, **** indicates $P < 0.0001$, *** indicates $p < 0.001$, ** indicates $p < 0.01$, and * indicates $p < 0.05$.

Data representation

When box-and-whisker graphs are plotted, the middle line represents the median value of the sample. The color box extremities represent the first and the third quartile. The whisks represent both the minimum and maximum bounds of the sample. When a histogram bar graph was plotted, values shown in the text and figures are mean and standard deviation (SD).

References

1. Cohen, S., Valm, A. M. & Lippincott-Schwartz, J. Interacting organelles. *Current opinion in cell biology* **53**, 84–91 (2018).
2. Valm, A. M. *et al*. Applying systems-level spectral imaging and analysis to reveal the organelle interactome. *Nature* **546**, 162–167 (2017).
3. Baumgart, T. *et al*. Large-scale fluid/fluid phase separation of proteins and lipids in giant plasma membrane vesicles. *Proceedings of the National Academy of Sciences* **104**, 3165–3170 (2007).
4. Sezgin, E. *et al*. Elucidating membrane structure and protein behavior using giant plasma membrane vesicles. *Nature protocols* **7**, 1042–1051 (2012).
5. Santinho, A. *et al*. Membrane Curvature Catalyzes Lipid Droplet Assembly. *Current Biology* **30**, 2481-2494.e6 (2020).
6. King, C., Sengupta, P., Seo, A. Y. & Lippincott-Schwartz, J. ER membranes exhibit phase behavior at sites of organelle contact. *Proceedings of the National Academy of Sciences* (2020).
7. Jaiswal, A., Hoerth, C. H., Pereira, A. M. Z. & Lorenz, H. Improved spatial resolution by induced live cell and organelle swelling in hypotonic solutions. *Scientific reports* **9**, 1–13 (2019).
8. Upadhyaya, A. & Sheetz, M. P. Tension in tubulovesicular networks of Golgi and endoplasmic reticulum membranes. *Biophysical journal* **86**, 2923–2928 (2004).
9. Dezi, M., Di Cicco, A., Bassereau, P. & Lévy, D. Detergent-mediated incorporation of transmembrane proteins in giant unilamellar vesicles with controlled physiological contents. *Proceedings of the National Academy of Sciences* **110**, 7276–7281 (2013).
10. Joshi, A. S., Zhang, H. & Prinz, W. A. Organelle biogenesis in the endoplasmic reticulum. *Nature cell biology* **19**, 876 (2017).
11. Voeltz, G. K., Prinz, W. A., Shibata, Y., Rist, J. M. & Rapoport, T. A. A class of membrane proteins shaping the tubular endoplasmic reticulum. *Cell* **124**, 573–586 (2006).
12. Wu, H., Carvalho, P. & Voeltz, G. K. Here, there, and everywhere: The importance of ER membrane contact sites. *Science* **361**, (2018).
13. Prasad, R., Sliwa-Gonzalez, A. & Barral, Y. Mapping bilayer thickness in the ER membrane. *Science advances* **6**, eaba5130 (2020).
14. Colom, A. *et al*. A fluorescent membrane tension probe. *Nature chemistry* **10**, 1118–1125 (2018).
15. Danylchuk, D. I., Jouard, P.-H. & Klymchenko, A. S. Targeted solvatochromic fluorescent probes for imaging lipid order in organelles under oxidative and mechanical stress. *Journal of the American Chemical Society* **143**, 912–924 (2021).
16. Chen, F., Tillberg, P. W. & Boyden, E. S. Expansion microscopy. *Science* **347**, 543–548 (2015).
17. Christopher, J. A. *et al*. Subcellular proteomics. *Nature Reviews Methods Primers* **1**, 1–24 (2021).
18. Sezgin, E., Levental, I., Mayor, S. & Eggeling, C. The mystery of membrane organization:

composition, regulation and roles of lipid rafts. *Nat Rev Mol Cell Biol* **18**, 361–374 (2017).
19. Lorent, J. H. *et al*. Plasma membranes are asymmetric in lipid unsaturation, packing and protein shape. *Nature chemical biology* **16**, 644–652 (2020).
20. Sych, T., Levental, K. R. & Sezgin, E. Lipid–Protein Interactions in Plasma Membrane Organization and Function. *Annual Review of Biophysics* **51**, (2022).
21. Rawicz, W., Olbrich, K. C., McIntosh, T., Needham, D. & Evans, E. Effect of chain length and unsaturation on elasticity of lipid bilayers. *Biophysical journal* **79**, 328–339 (2000).
22. Shibata, Y. *et al*. Mechanisms determining the morphology of the peripheral ER. *Cell* **143**, 774–788 (2010).
23. Steinkühler, J., Sezgin, E., Urbančič, I., Eggeling, C. & Dimova, R. Mechanical properties of plasma membrane vesicles correlate with lipid order, viscosity and cell density. *Communications biology* **2**, 1–8 (2019).
24. Santinho, A., Chorlay, A., Foret, L. & Thiam, A. R. Fat Inclusions Strongly Alter Membrane Mechanics. *Biophysical Journal* (2021).
25. Pinot, M. *et al*. Polyunsaturated phospholipids facilitate membrane deformation and fission by endocytic proteins. *Science* **345**, 693–697 (2014).
26. Levental, K. R. *et al*. Lipidomic and biophysical homeostasis of mammalian membranes counteracts dietary lipid perturbations to maintain cellular fitness. *Nature communications* **11**, 1–13 (2020).
27. Halbleib, K. *et al*. Activation of the unfolded protein response by lipid bilayer stress. *Molecular cell* **67**, 673–684 (2017).
28. Koh, J. H., Wang, L., Beaudoin-Chabot, C. & Thibault, G. Lipid bilayer stress-activated IRE-1 modulates autophagy during endoplasmic reticulum stress. *Journal of cell science* **131**, jcs217992 (2018).
29. Ben M'barek, K. *et al*. ER Membrane Phospholipids and Surface Tension Control Cellular Lipid Droplet Formation. *Dev. Cell* **41**, 591-604.e7 (2017).
30. Chung, J. *et al*. LDAF1 and Seipin Form a Lipid Droplet Assembly Complex. *Developmental Cell* (2019).
31. Zoni, V. *et al*. Seipin accumulates and traps diacylglycerols and triglycerides in its ring-like structure. *Proceedings of the National Academy of Sciences* **118**, (2021).
32. Prasanna, X. *et al*. Seipin traps triacylglycerols to facilitate their nanoscale clustering in the endoplasmic reticulum membrane. *PLoS biology* **19**, e3000998 (2021).
33. Thiam, A. R. & Ikonen, E. Lipid Droplet Nucleation. *Trends in Cell Biology* (2020).
34. Choudhary, V., El Atab, O., Mizzon, G., Prinz, W. A. & Schneiter, R. Seipin and Nem1 establish discrete ER subdomains to initiate yeast lipid droplet biogenesis. *Journal of Cell Biology* **219**, (2020).
35. Salo, V. T. *et al*. Seipin facilitates triglyceride flow to lipid droplet and counteracts droplet ripening via endoplasmic reticulum contact. *Developmental cell* **50**, 478–493 (2019).
36. Cartwright, B. R. *et al*. Seipin performs dissectible functions in promoting lipid droplet biogenesis and regulating droplet morphology. *Molecular biology of the cell* **26**, 726–739 (2015).